One gene, two diseases and three conformations: Molecular dynamics simulations of mutants of human prion protein at room temperature and elevated temperatures

ARTICLE *in* PROTEINS STRUCTURE FUNCTION AND BIOINFORMATICS · MAY 2005

Impact Factor: 2.63 · DOI: 10.1002/prot.20401 · Source: PubMed

2 AUTHORS:

Shahir Shamsir
Universiti Teknologi Malaysia
77 PUBLICATIONS **119** CITATIONS
SEE PROFILE

Andrew R Dalby
University of Westminster
29 PUBLICATIONS **596** CITATIONS
SEE PROFILE

One Gene, Two Diseases and Three Conformations: Molecular Dynamics Simulations of Mutants of Human Prion Protein at Room Temperature and Elevated Temperatures

Mohd S. Shamsir and Andrew R. Dalby*

Schools of Biological and Chemical Sciences and Engineering and Computer Science, University of Exeter, Washington Singer Laboratories, Prince of Wales Road, Exeter

ABSTRACT **Fatal familial insomnia (FFI) and Creutzfeldt-Jakob disease (CJD) are associated to the same mutation at codon 178 but differentiate into clinicopathologically distinct diseases determined by this mutation and a naturally occurring methionine–valine polymorphism at codon 129 of the prion protein gene. It has been suggested that the clinical and pathological difference between FFI and CJD is caused by different conformations of the prion protein. Using molecular dynamics (MD), we investigated the effect of the mutation at codon 178 and the polymorphism at codon 129 on prion protein dynamics and conformation at normal and elevated temperatures. Four model structures were examined with a focus on their dynamics and conformational changes. The results showed differences in stability and dynamics between polymorphic variants. Methionine variants demonstrated a higher stability than valine variants. Elongation of existing β-sheets and formation of new β-sheets was found to occur more readily in valine polymorphic variants. We also discovered the inhibitory effect of proline residue on existing β-sheet elongation. Proteins 2005;59:275–290.** © 2005 Wiley-Liss, Inc.

INTRODUCTION

Prions and Prion Diseases

Human transmissible spongiform encephalopathies (TSE), commonly known as prion diseases, include diseases such as Kuru, Creutzfeldt-Jakob disease (CJD), Gerstmann-Straussler-Sheinker syndrome, and fatal familial insomnia (FFI). These are rare and fatal neurodegenerative conditions that occur as familial, infectious, or sporadic diseases.[1]

The human prion protein is a product of a single host gene (PRNP) located on the short arm of chromosome 20. The sequence of the translated product is 253 amino acids long, including two signal sequences in the amino- and carboxy-terminal ends that are removed during post-translational modification. Prion protein contains five amino-terminal octapeptide repeats, two glycosylated sites at Asn181 and Asn197,[2] and one disulfide bridge between Cys179 of the second helix and Cys214 of the third helix.[3] The protein is known to be membrane associated, as there is a glycosylphosphatidylinositol anchor at its C-terminal Ser231, which attaches the protein to the outer surface of the cell membrane.[4]

The precise function of PrP^C is yet to be fully determined, and the absence of gross phenotype alteration in PrP^C-null mice makes this increasingly difficult. The presence of an octapeptide repeat, which binds to copper, suggests a role in copper metabolism, as cultured PrP^C-deficient cells have been shown to have a reduced copper content, lower superoxide dismutase activity and increased susceptibility to oxidative stress.[5] In addition, PrP^C-null mice show increased protein and lipid oxidation.[6] Active uptake of PrP^C by clathrin-coated pits[7] and caveolae-like vesicles[8] suggests a role in copper homeostasis by means of a copper sink or as a carrier for other copper-requiring cytosolic proteins. There is a notable abundance of PrP^C in the hippocampus, a region thought to be involved in memory function, suggesting a role in memory formation for PrP^C.[9,10] Another suggested function derived from neuronal studies on cells from PrP-null mice is neuroprotection.[11]

The nuclear magnetic resonance (NMR) structure of the mature recombinant human prion protein predicts an orthogonal bundle (OB)[12] structured globular domain extending from residues 125 to 228 and an N-terminal flexible and disordered region. The globular domain contains three α-helices comprising residues 144–154 (H1), 173–194 (H2), and 200–228 (H3) and an anti-parallel β-sheet consisting of two short strands comprising residues 128–131 (S1) and 161–164 (S2).[13,14]

Abbreviations: CJD, Creutzfeldt-Jakob disease; DM, native methionine polymorphism of PrP; DV, native valine polymorphism of PrP; FFI, fatal familial insomnia; MD, molecular dynamics; NM, methionine polymorphism of PrP D178N mutant; NMR, nuclear magnetic resonance; NV, valine polymorphism of PrP D178N mutant; PrP, prion protein; PrP^C, prion protein cellular form; PrP^{SC}, prion protein scrapie form; TSE, transmissable spongeiform encephalopathies

*Correspondence to: Andrew Dalby, School of Biological and Chemical Sciences and Engineering and Computer Science, University of Exeter, Washington Singer Laboratories, Perry Road, Prince of Wales Road, Exeter EX4 4QG, UK. E-mail: a.r.dalby@exeter.ac.uk

Received 20 July 2004; Revised 27 September 2004; Accepted 4 October 2004

Published online 28 February 2005 in Wiley InterScience (www.interscience.wiley.com). DOI: 10.1002/prot.20401

TABLE I. Clinicopathological Differences Between CJD and FFI

	Diagnostic Symptoms	Onset	Degeneration	Duration of Illness	Clinical Evolution
CJD	Dementia, ataxia, dysphasia myoclonus,	60–70 years	Cerebral cortex	Short	Rapid
FFI	Insomnia, dysautonomia, pyrexia hyperhydrosis,	30–40 years	Thalami	Long	Slow

According to the 'prion only' hypothesis, the key event of prion pathogenesis in TSE diseases is the conformational conversion of the prion protein (PrP) from its normal isoform (PrP^{C}) to a diseased scrapie isoform (PrP^{SC}). This purely conformational transition results in changes in four properties;[15]

1. Increase in the β sheet content from 3 to 43%.
2. Reduction of the α-helical content from 42 to 30%.[16]
3. Decrease in solubility.
4. Increased resistance to proteases.[17]

Although PrP^{SC} itself is not neurotoxic, aggregation and accumulation of PrP^{SC}, coupled with the loss of PrP^{C} functions, has been shown to cause an increase in oxidative stress and mitochodrial dysfunction[18] and to disrupt iron[19] and calcium homeostasis.[20,21] These aggravating factors may subsequently cause the triggering of the apoptotic pathway and neurodegeneration found in TSE diseases.[22–25] This is in stark contrast to the recently reported role of PrP^{C} in protecting against apoptosis in serum deprivation studies.[26]

Polymorphism in Prion Diseases

FFI and CJD, two clinicopathologically distinct diseases, are associated with the same mutation at codon 178.[27,28] A GAC-to-AAC mutation of PRNP at codon 178 causes a substitution of aspartic acid with asparagine (D178N). CJD, first described in 1920, is the most common clinicopathological subtype of human prion disease[29] and exists in four subtypes that are defined by their causative mechanisms and clinicopathology (Table I).[30] Clinical symptoms associated with CJD are dementia, myoclonus, and spongiform degeneration in the cerebral cortex.[23] FFI was categorized as a prion disease in 1992[27] and is characterized clinically by a loss of the ability to sleep, dysautonomia, and selective atrophy of thalami.[29] The main differences in the pathological pattern between CJD and FFI are summarized in Table II.

Segregation of CJD and FFI into distinct phenotypic expressions is determined by both the D178N mutation and the naturally occurring methionine–valine polymorphism at codon 129 (c129) (Fig. 1) of the prion protein gene.[31] The c129 PRNP codon influences the susceptibility and phenotype of the disease. For example, homozygosity in the prion protein genotype predisposes the individual with the D178N mutation to either FFI (NM) or CJD (NV).[32] Interestingly, all of the new variant CJD (vCJD) subjects to date are homozygous methionine, which would normally be associated with FFI.[33]

The abnormal protease-resistant forms of the prion protein in these two diseases were found to differ both in the relative abundance of glycosylated forms and in the size of the protease-resistant fragments. This is consistent with a different protease cleavage site in the two diseases, where the deglycosylated prion associated with the CJD phenotype is approximately 21 kDa, while that associated with FFI is 19 kDa.[34] Differences also exist between the cellular metabolism of NM and D178V when transfected to human neuroblastoma cells.[35] The D178N mutation is shown to cause instability of the mutant PrP, which is partially corrected by N–glycosylation. Hence, only the glycosylated forms of D178N mutant PrP reach the cell surface, whereas the unglycosylated form is degraded. However, further studies have shown overlapping clinicopathological diversity, which suggests that previous results were artifacts of phenotypic studies.[36] The presence of this broad pathological heterogeneity overlapping in both diseases casts a degree of uncertainty on the claim that the ultimate phenotype is determined entirely by associated c129 allelic polymorphism.

TABLE II. Different Forms of CJD

Types	Notes
Sporadic	Random worldwide distribution: approximately one case per million per year
Genetic/familial	Associated with PRNP mutations; autosomal dominant
Iatrogenic	Acquired through dura mater grafts, surgery, and hormone treatments
Variant	Linked to bovine spongiform encephalopathies

The aim of these simulations was to investigate the influence of polymorphism on the globular domain of the prion protein, particularly the effects on protein stability and unfolding dynamics. High-temperature simulations were used to bring about the unfolding of the globular domain. By increasing temperature, protein unfolding can be accelerated without changing the pathway of unfolding, and this enables the elucidation of the protein unfolding pathway at minimal computational expense.[37] Previous MD simulations on D178N mutants were performed on a different point mutation[38] and at a lower temperature.[39] We chose to simulate only the globular domain of PrP^{C}, as this shorter fragment has been detected in PrP^{SC}-infected brains,[40] and because of the absence of reliable structural data that include residues 90–124.

MATERIALS AND METHODS

The initial structures for all of the simulations were based on the NMR structure of human prion protein

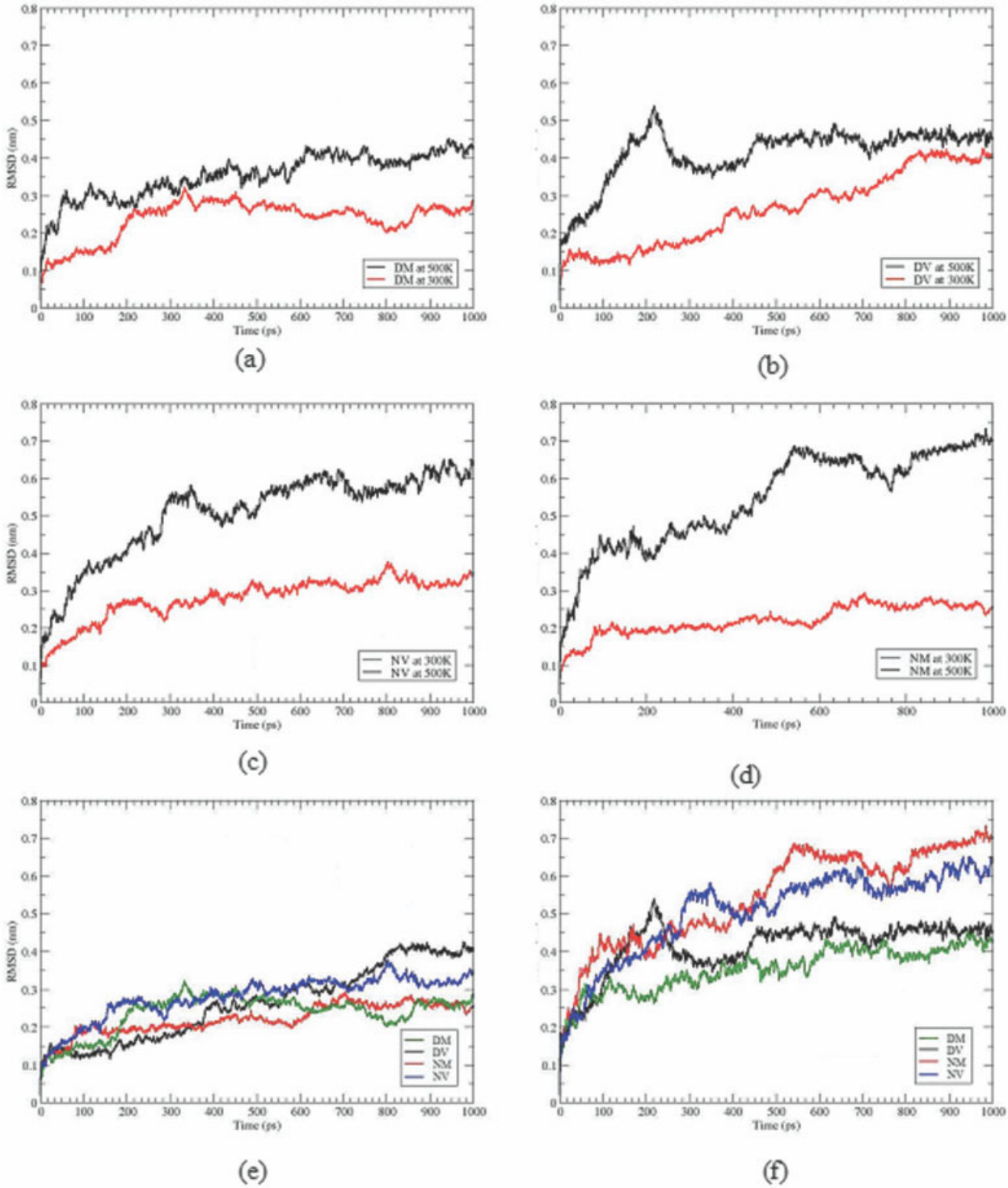

Fig. 2. RMSD of polymorphic variants and mutants: (**a**) native methionine (DM); (**b**) native valine (DV); (**c**) valine polymorphic variant with D178N mutant associated with CJD (NV); (**d**) methionine polymorphic variant with D178N mutant associated with FFI (NM); (**e**) RMS of all variants at 300K (black: DV, green: DM, blue: NV, red: NM); (**f**) RMS of all variants at 500K.

domain in the Protein Data Bank[41] designated 1QLX,[14] which contains the C-terminal globular structure of human prion consisting of residues 125–228. Polymorphic and mutant structures were constructed using Deep View[42] by substituting Met with Val at position 129 and substituting Asp with Asn at position 178. Four variants were used for the simulations: native Met (DM), native Val (DV), NM and NV. The disulfide bond between H2 and H3 was left intact, as previous work showed that it remains oxidized in PrP^{SC} and necessary for infectivity.[3,43] Residue numbers

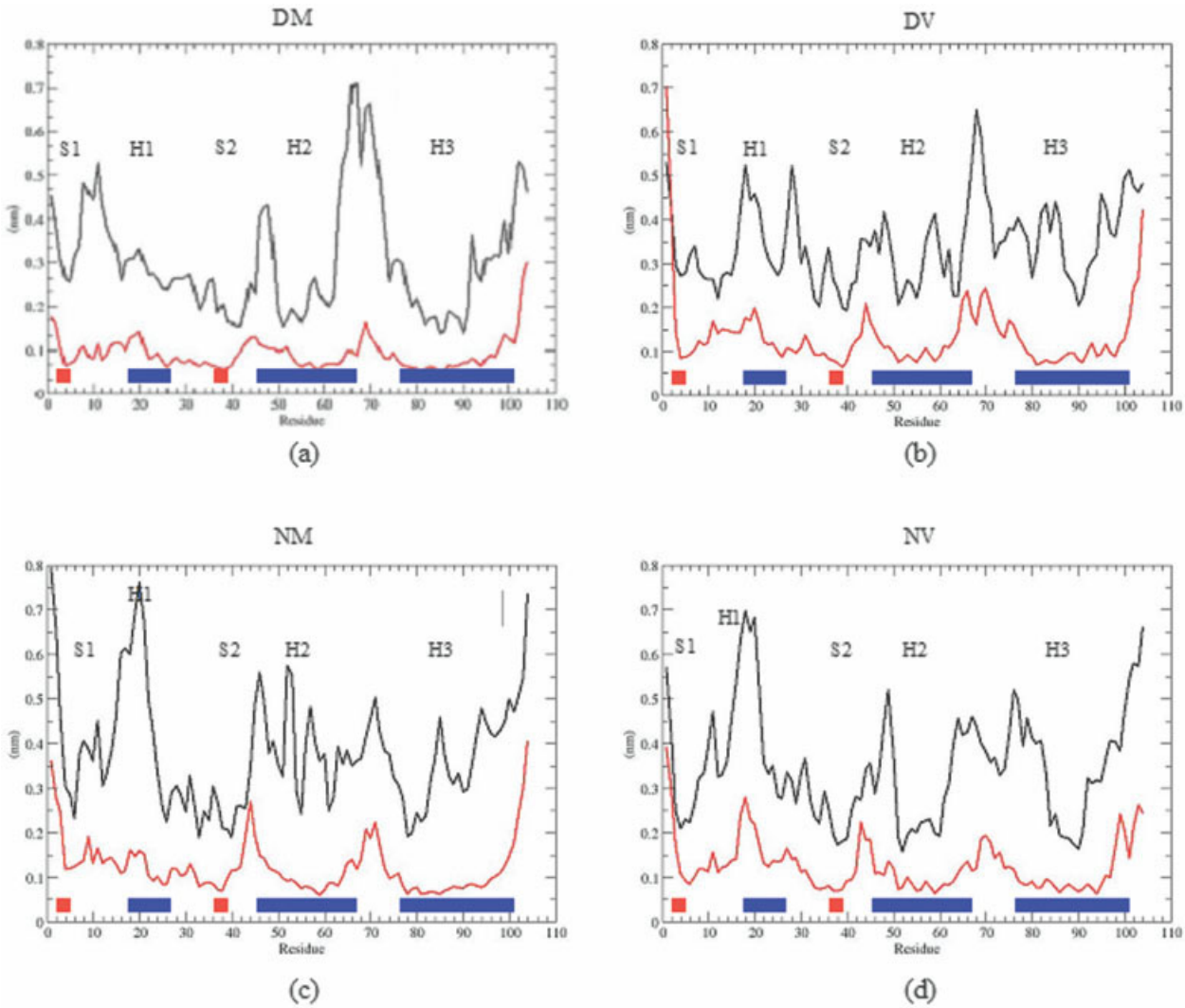

Fig. 3. RMS fluctuations of polymorphic variants and mutants at 300 and 500K: (**a**) DM (**b**) DV (**c**) NM (**d**) NV. Red lines denote fluctuations at 300K, black lines at 500K; blue bars denote α-helices, red bars β-sheets; S1, sheet 1; S2, sheet 2; H1, helix 1; H2, helix 2; H3, helix 3. (**e**) Ribbon diagram of human prion 1QLX with secondary structures (red: helices, yellow: sheets); dark blue, Asp178; light blue, Tyr128; green, Arg164 (see next page).

were changed from 125–228 to 0–103. All models were solvated in a box of explicit simple point charge (SPC) water molecules and simulated using periodic boundary conditions. Structures were minimized using 200 steps of the steepest descent method. Simulations were performed using GROMACS 3.1.4 package and the all-hydrogen function GROMOS96.[44] The temperature was maintained at 300 and 500K, and isotropic pressure coupling was applied. All systems were equilibrated for 200 ps of solute position-restrained MD. Unrestrained MD were performed for 1 ns with a LINCS algorithm 2 fs time step for each system. Simulations were performed at pH 7. The temperature 500K, chosen as the high temperature, has been shown to accelerate the process of protein unfolding while preserving the protein unfolding pathway.[37] Previous simulations at higher temperatures[45,46] have shown the preservation of secondary structures at elevated temperatures, and experimental results have shown that temperatures in excess of 394–410K are required to inactivate prion protein.[47,48] Simulations were repeated three times with different starting velocities and showed a high degree of reproducibility, especially in the case of NM. All of the resulting trajectories were analyzed using GROMACS utilities, and results are given for a representative trajectory. The C_α root mean square deviations (RMSD) and C_α root mean square fluctuations (RMSF) relative to the average MD structure were calculated. The DSSP[49] program was used to determine the percentage of secondary structure throughout the simulations. Protein structure images were created using PyMOL[50] and Protein Explorer.[51]

RESULTS AND DISCUCION

Structural Deviations

Figure 2(a–d) shows the RMS positional deviations from the NMR structure as functions of simulation time for the C_α atom in each polymorphic variant. Figure 2(e,f) shows a

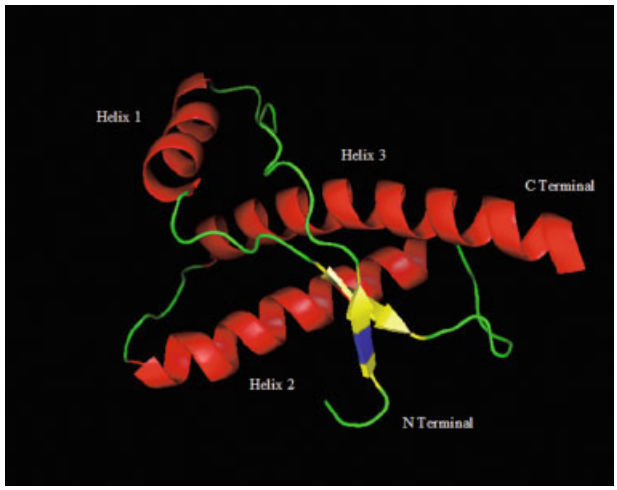

Fig. 1. Ribbon diagram of human prion 1QLX with secondary structures (red: helices, yellow: sheets) and codon 129 (blue).

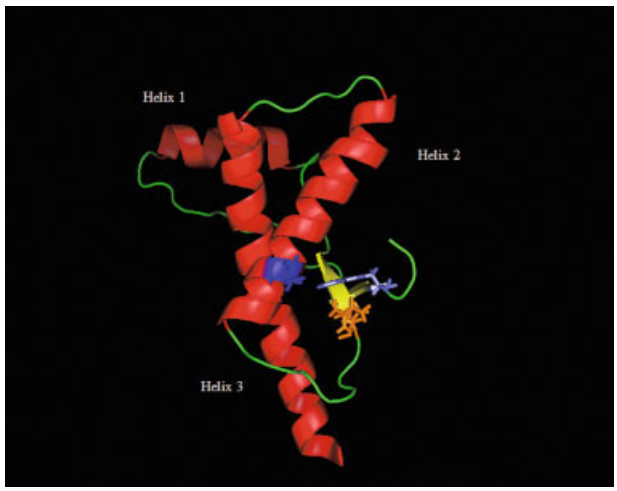

Figure 3. (Continued.)

Fig. 10. Ribbon diagram of human prion 1QLX with secondary structures (red: helices, yellow: sheets) and proline residues numbered in stick form and highlighted in white.

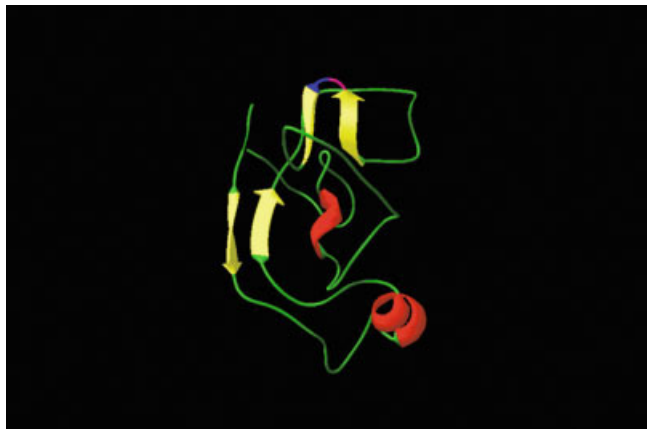

Fig. 11. Ribbon diagram of NM with secondary structures (red: helices, yellow: sheets) and Thr183 (pink) and Ile184 (blue).

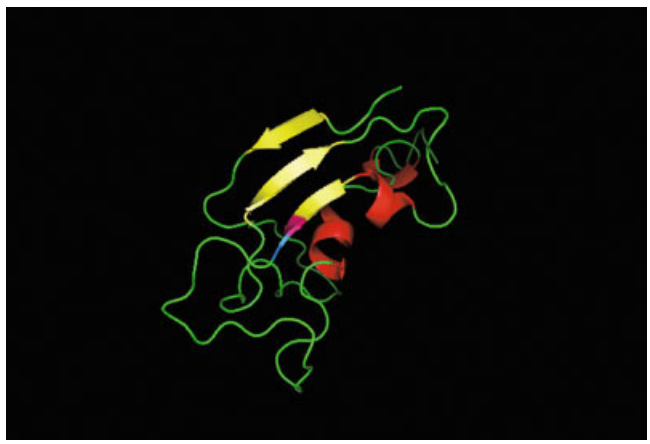

Fig. 12. Ribbon diagram of NV with secondary structures (red: helices, yellow: sheets) and Thr183 (pink) and Ile184 (blue).

comparison between residues at 300 and 500K respectively.

In the simulations at 300K, the C_α RMSD values for both normal and mutant polymorphic variants remain relatively low, although DV deviates more from the initial structure than DM. The RMSD plot reaches a plateau at similar times for both polymorphic variants. In both normal and mutant methionine polymorphic variants, the RMSD plot plateaus early, at 0.2 and 0.1 ns, respectively, with an average value of 0.25 $\pm$ 0.05 nm. In contrast, for both normal and mutant valine polymorphic variants, the RMSD plot plateaus later, at 0.8 and 0.6 ns, respectively, with an average value of 0.4 $\pm$ 0.05 nm and 3.0 $\pm$ 0.05 nm respectively. Overall, valine variants DV and NV have higher RMSD values than methionine variants DM and NM.

In simulations at 500K, the mutant variants deviate further from the average NMR structure than their normal polymorphic variants [Fig. 2(f)]. The RMSD of DM and DV structures in the last 200 ps are 0.4 $\pm$ 0.05 nm and 0.45 $\pm$ 0.05 nm respectively, while NM and NV RMSD values are 0.6 $\pm$ 0.05 nm and 0.7 $\pm$ 0.05 nm respectively. The RMSD values of each variant increase

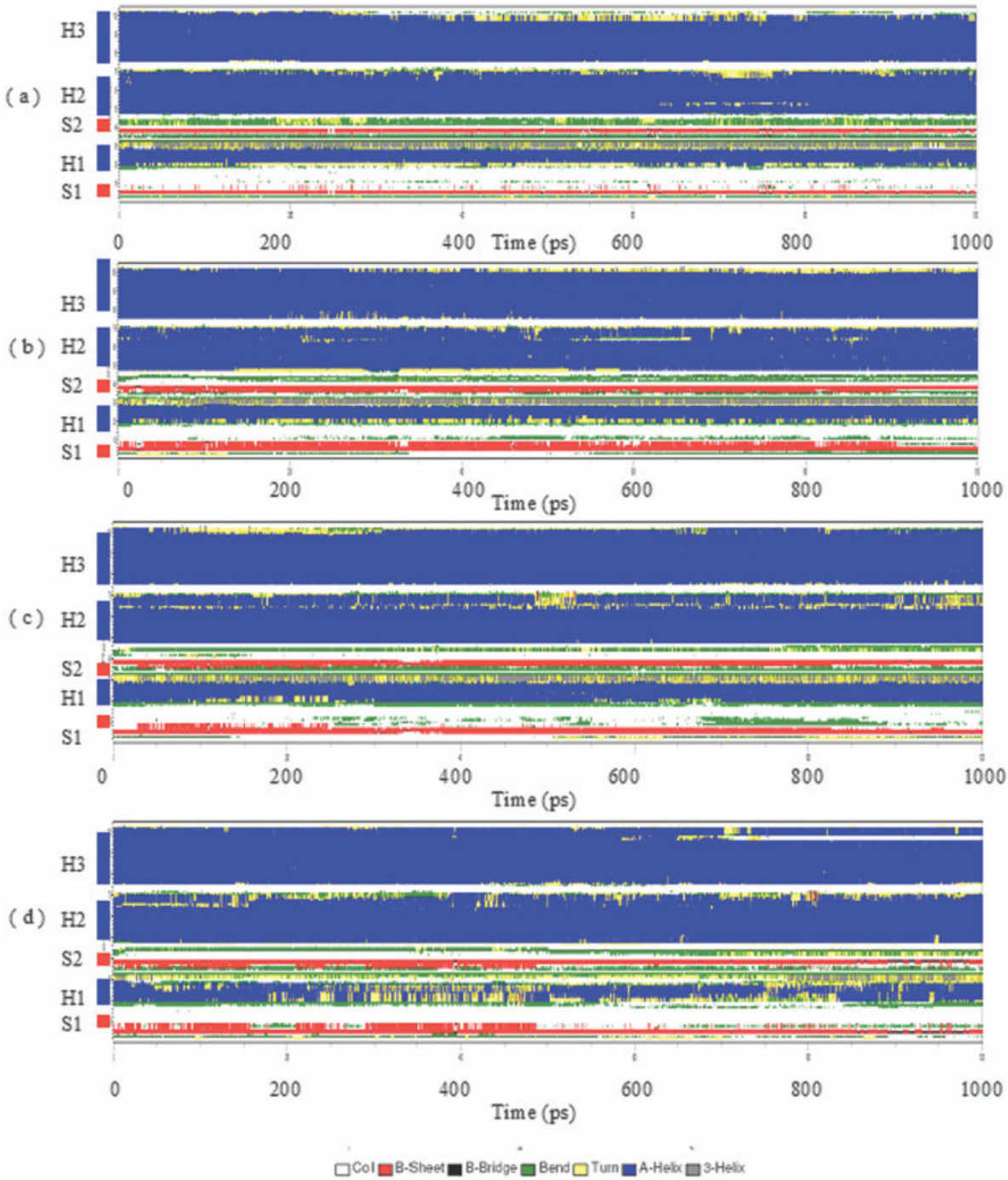

Fig. 4. Secondary structure as a function of simulation time determined with DSSP at 300K: (**a**) DM, (**b**) DV, (**c**) NM, (**d**) NV mutant associated with FFI; S1, sheet 1; S2, sheet 2; H1, helix 1; H2, helix 2; H3, helix 3. The color guide designates types of secondary structure.

at a similar rate to each other until 100 ps, after which the values for mutant variants increase faster than those for native variants. Although the final RMSD values of DM and DV are similar, RMSD values for DM increase at an almost constant rate to reach the final value; in contrast, DV shows an initial rapid increase during the first 200 ps followed by a drop and plateau of RMSD value. This rapid increase of RMSD is attributed to rapid unwinding of H3 of DV during the first 200 ps [Fig. 2(b)].

Structural Fluctuations

Figure 3(a–d) shows the RMSF of C_α atoms as a function of residue number. Each simulation at 300K follows a groove pattern found in previously published molecular simulations,[45,52,53] where DM showed the lowest fluctua-

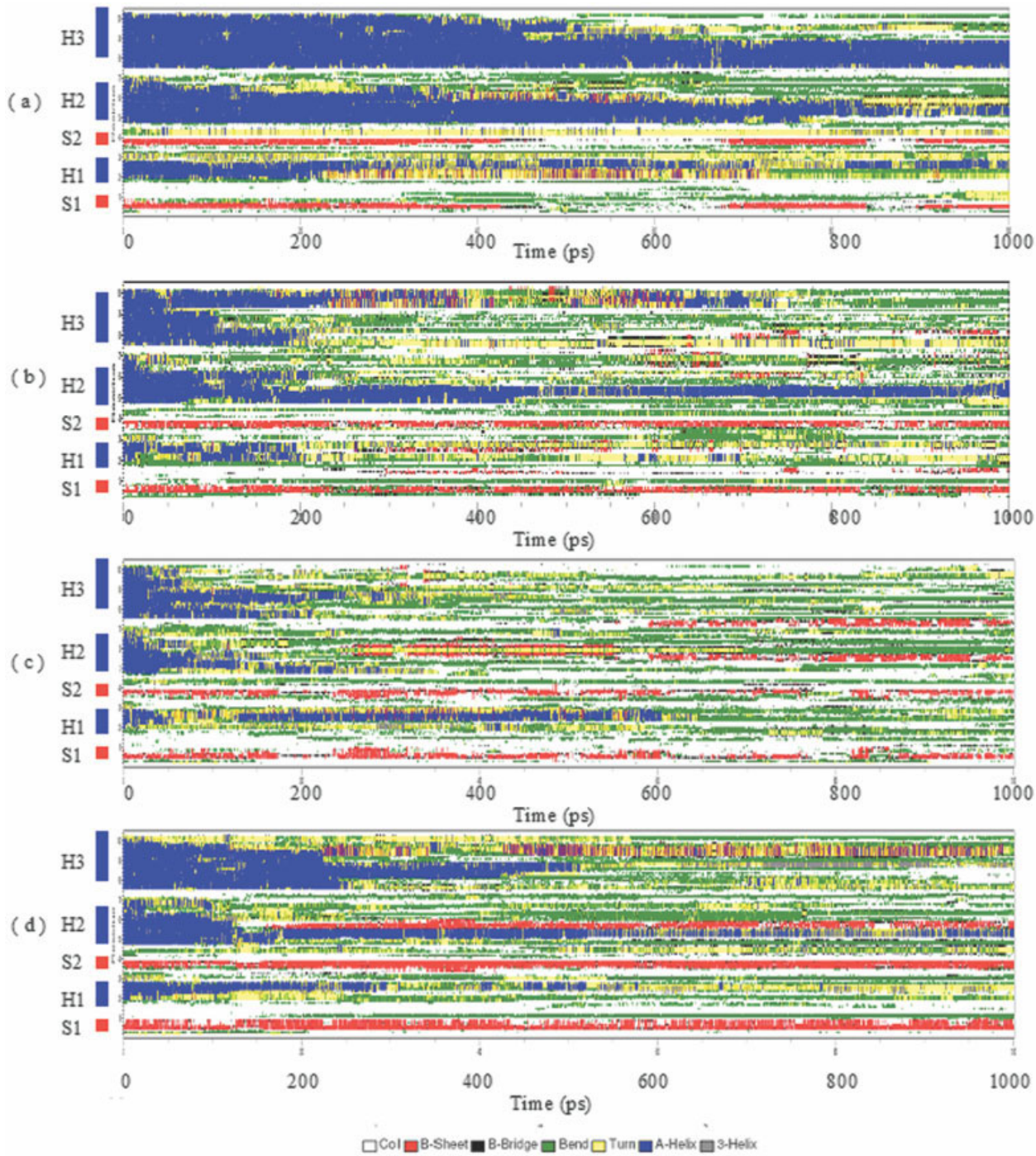

Fig. 5. Secondary structure as a function of simulation time determined with DSSP at 500K: (**a**) DM, (**b**) DV, (**c**) NM, (**d**) NV mutant associated with FFI; S1, sheet 1; S2, sheet 2; H1, helix 1; H2, helix 2; H3, helix 3. The color guide designates types of secondary structure.

tion compared to the rest. In addition to the anticipated flexibility of the N- and C-termini of the globular domain at 300K, fluctuations occurred at the loop before H2 (165–172) and the loop before H3 (193–199) at 300K. The lowest fluctuations were observed in the region of the disulfide bridge (residue 154).

The RMSF of C_α atoms at 500K in Figure 4(a–d) shows an increase in fluctuation. The RMSF of DM at 500K conforms relatively closely to its previous RMSF at 300K, indicating a relatively high structural rigidity compared to DV, NM, and NV. Comparative mutant studies have shown that substitution mutations in prion protein reduce thermodynamic stability.[54] In the case of D178N, the substitution of Asp 178 with Asn in NM and NV affects a solvent-accessible bridge of Arg164 to Asp178 and a hydrogen bond between Tyr128 and Asp 178. This isosteric alteration destabilizes the protein by

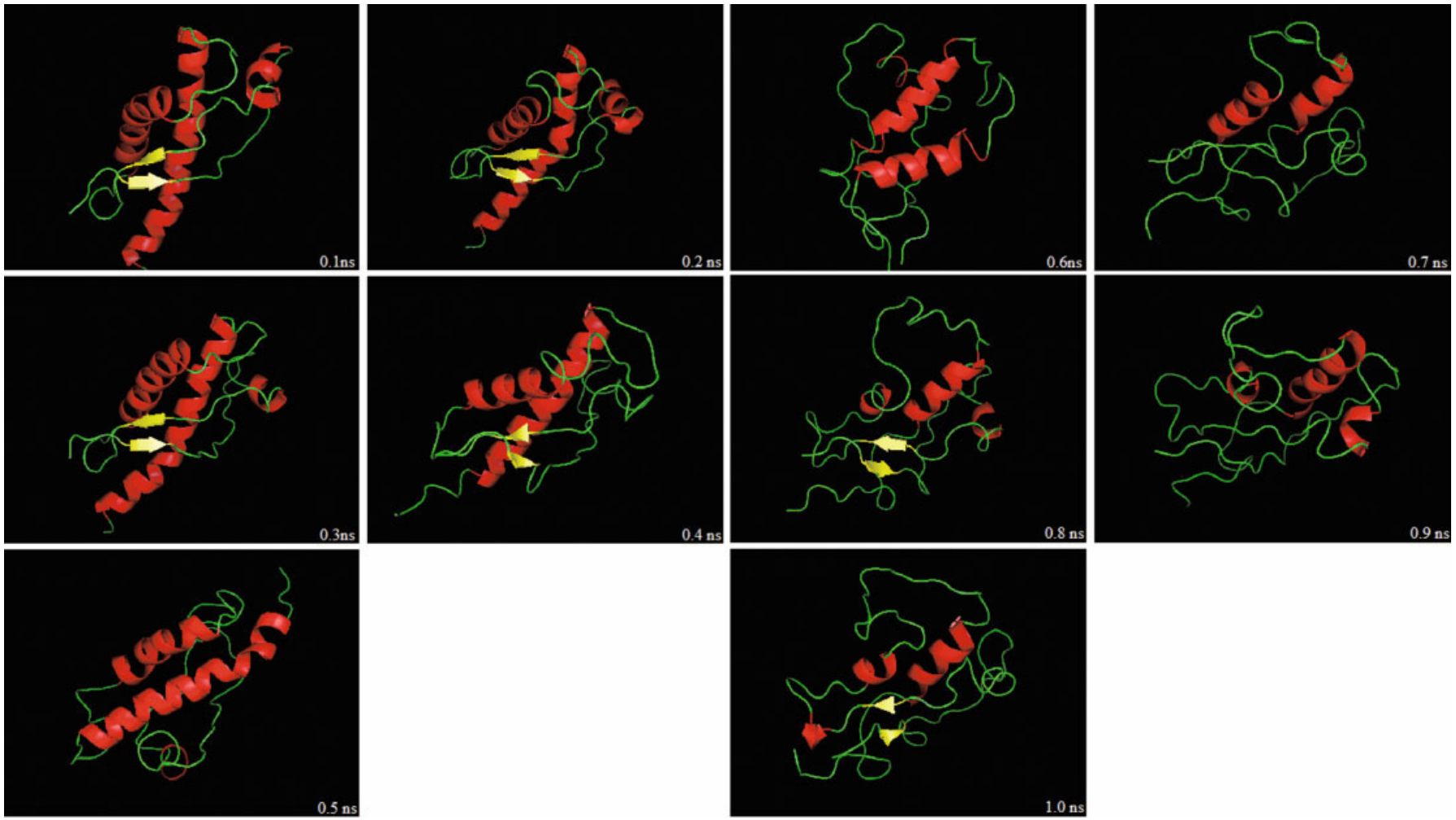

Fig. 6. Temporal evolution snapshots of DM taken between (**A**–**E**) 0.1 and 0.5 ns and (**F**–**J**) 0.6 and 1.0 ns at 0.1-ns intervals at 500K.

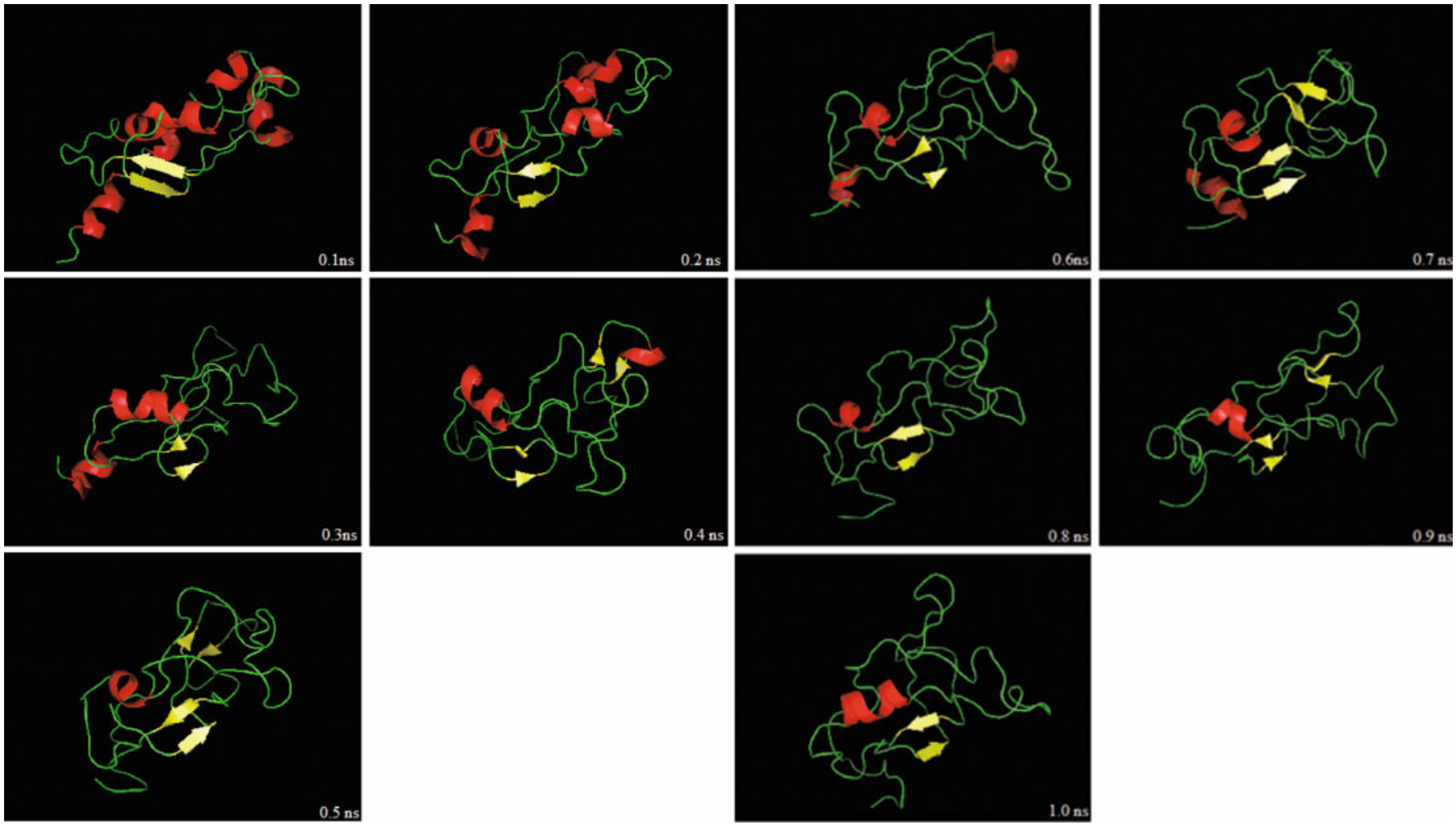

Fig. 7. Temporal evolution snapshots of DV taken between (**A**–**E**) 0.1 and 0.5 ns and (**F**–**J**) 0.6 and 1.0 ns at 0.1-ns intervals at 500K.

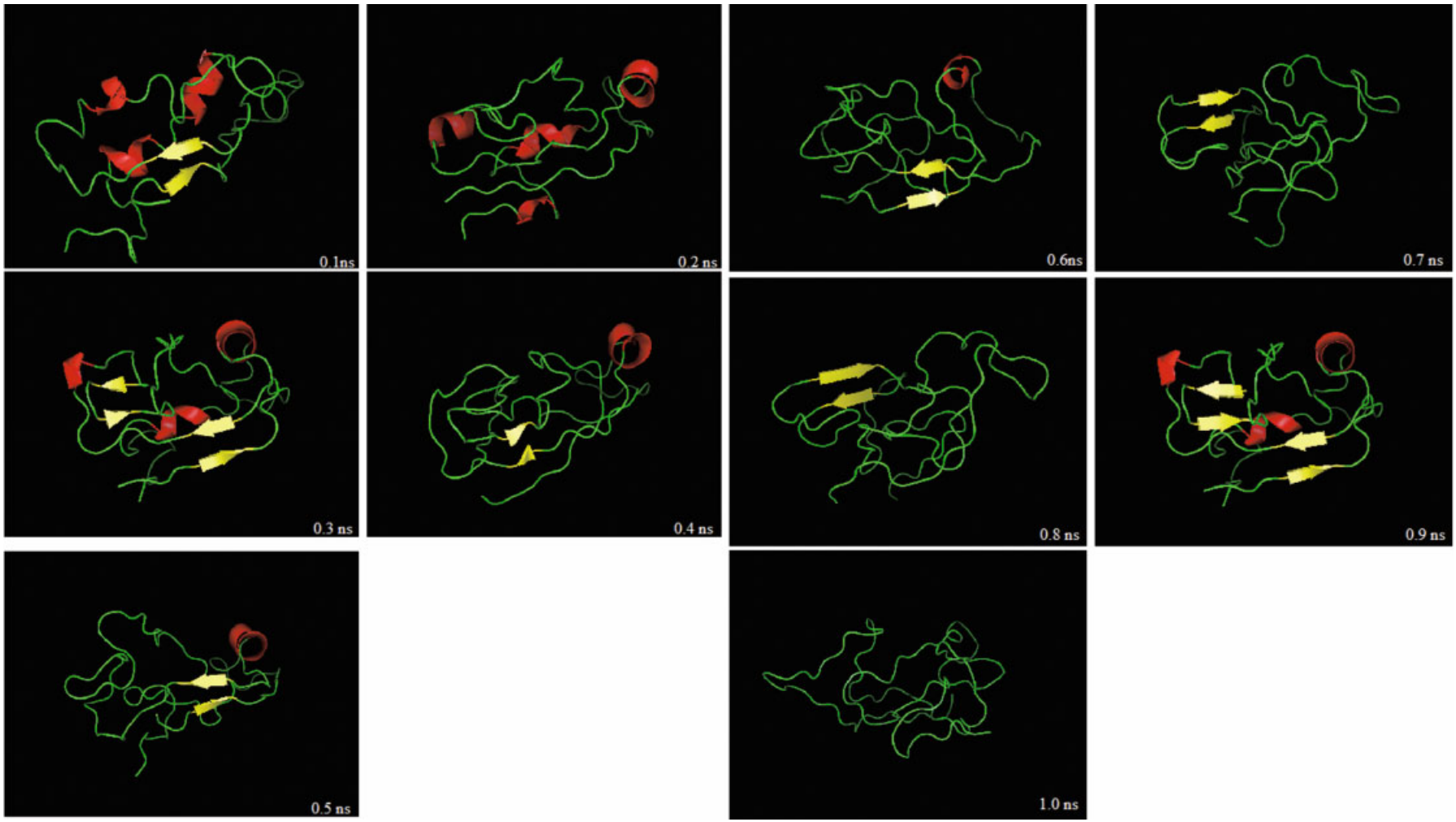

Fig. 8. Temporal evolution snapshots of NM taken between (**A**–**E**) 0.1 and 0.5 ns and (**F**–**J**) 0.6 and 1.0 ns at 0.1-ns intervals at 500K.

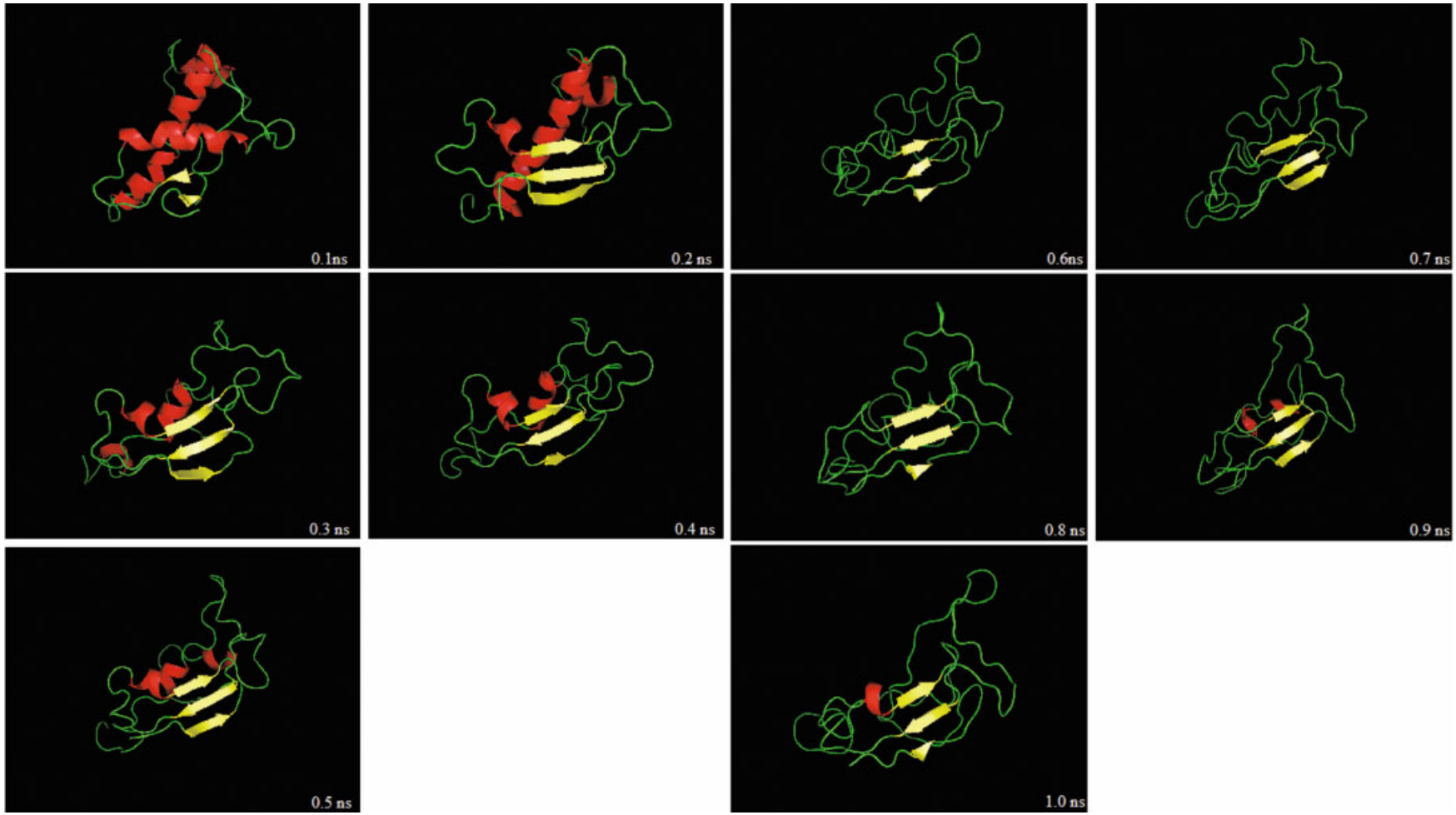

Fig. 9. Temporal evolution snapshots of NV taken between (**A**–**E**) 0.1 and 0.5 ns and (**F**–**J**) 0.6 and 1.0 ns at 0.1-ns intervals at 500K.

7-8 kJ/mol, which may rearrange the conformation between the β-sheets and H2 [Fig. 3(e)]. The increase of fluctuations and dynamics in simulations at 500K demonstrates the decreased stability of D178N mutant variants. The absence of observable fluctuation differences between NM and NV conforms with thermodynamic stability studies using urea-induced unfolding/refolding experiments, which suggests that neither Met nor Val at residue 129 has an influence on the D178N mutation.[54] Interestingly, DV shows similar increased fluctuations to NM and NV. Therefore, the elevated DV dynamics during the simulation suggests a difference in conformational stability between Met and Val PrP^C variants.

Structural Evolution

Preservation of structure

Simulations at 300K showed preservation of prion protein tertiary structure in all the variants throughout the simulation. Increased fluctuations were observed in the rest of the variants compared to DM, especially in the highly mobile regions between helices. The two β-strands and helices 2 and 3 form a stiffer scaffold [Fig 3(a–d)]. Although there was increased mobility, there were no significant structural differences among DM, DV, NM, and NV at the end of the simulations. It is anticipated that there would be no significant modifications of the tertiary structure (e.g. different global fold or major alterations in the secondary structure) as mutant protein occurs naturally and allows a normal life for carriers for more than five decades.[55] This also agrees with the results of near-ultraviolet (UV) spectroscopy studies that have shown the absence of significant conformational differences between mutated and normal prions.[54]

Unwinding of helices

Figure 4(a–d) shows the evolution of the secondary structures during the simulation at 300K as determined by DSSP.[49] The overall structure remains intact for both polymorphic variants. However, in the mutant proteins, there is a greater degree of fluctuation, resulting in the partial unwinding of H1 for NV [Fig. 4(d)]. Unwinding occurred at both ends, and the fluctuations show no discernible pattern. The only residues that did not unwind were residues Glu146 and Asp147, situated in the middle of the helix. Breaking up of the α-helix also occurred at 300K at residue His187 of the NM mutant. After energy minimization, H2 spanned from residue Asn173–Thr194. During the simulation, the helix broke at residue 187 into two helices spanning residues Asn173–Gln186 and Thr190–Thr194. The two interconnected helices differ in stability, as the first helix-spanning Asn173–Gln186 was stable throughout the simulation, while the second helix-spanning Thr190–Thr194 fluctuated and unwound [Fig 4(c)]. A previous study reported a similar break of prion H2 into two helices at residue Gln186.[56]

Figure 5(a–d) shows the evolution of DM, DV, NM, and NV at 500K respectively, and Figure 6(a–j), 7(a–j), 8(a–j), and 9(a–j) show snapshots of simulations taken at 0.1-ns intervals. In all simulations, H1 was the first to unwind compared to H2 and H3. Previous studies have suggested that the hydrophilicity of H1 makes it the most likely candidate to unwind and undergo an $\alpha \rightarrow \beta$ transition.[57] It has also been suggested that H1 is the least stable among the helices due to its lack of noncovalent contacts to the remainder of the protein and its apparently self-sustaining stabilization through the presence of intra-helix electrostatic interactions.[58] In every simulation, the unwinding of H1 occurred within the first 300 ps. This rapid unwinding during the simulation seems to confirm the unstable nature of H1 compared to H2 and H3. Overall, the denaturation rate was slowest in DM, followed by DV, NV, and NM.

Elongation and formation of new β-sheets

The $\alpha \rightarrow \beta$ conformational transition in PrP^C involves a 40% increase in β-sheet content in PrP^{SC}. This suggests that a relatively large number of residues in α-helices must unwind and rearrange into β-sheet conformation. Val has a higher β-sheet propensity than Met129,[59,60] which should influence the stability of the anti-parallel β-sheet spanning residues 128–131 and 161–164.

Elongation of β-sheets occurred at both 300 and 500K. At 300K, DV, NM, and NV undergo an extension of existing β-sheet spanning residues Met/Val129–Gly131 and Val161–Tyr163. The first sheet extended by two residues to Met/Val129–Ala133, while the second residue extended one residue to Gln160–Tyr163. This anti-parallel extension forms a G1 β-bulge that is found at the edges of anti-parallel β-sheets and is usually associated with β-hairpin turns.[61] There was no extension of β-sheets in DM throughout the simulation.

The elongation of existing β-sheets and the creation of new sheets in DV and in both mutants occurred in the 500K simulations [Fig. 5(b,–d)]. Elongation of sheets 1 and 2 occurred more significantly in the DV compared to NM and NV mutants. However, existing sheets did not elongate beyond Pro residues flanking both sides of sheet 2 (residues 158 and 165) and beyond Pro residue on the N-terminal end of sheet 1 (residue 137) (Fig. 10). This restrained elongation could be due to the presence of Pro, which disfavors β-sheets as it lacks one potential H-bond donor and its ϕ angle is not compatible with standard β-sheets.[62]

The transition of α-helices into β-sheets occurred within H2 of DV, NM, and NV mutants during the simulations. The formation occurred earliest in the NV at 150 ps [Fig. 5(d)], followed by NM [Fig. 5(c)] at 250 ps, and DV at 780 ps [Fig. 5(b)]. In NM, formation started with a turn at Thr183–Ile184, and an anti-parallel sheet formed between residues Val180, Asn 181, Ile 182 and Lys185, Gln186, His187 (Fig. 11). In NV, transition occurred at the same residues but without formation of the turn (Fig. 12). The sheet extended past Thr183–Ile184 and aligned anti-parallel with β-sheet 161–164. This conversion of α-helices to β-sheets within H2 could possibly be the trigger for the PrP^C to PrP^{SC} conformational change.[63,64]

Percentage of Secondary Structure

Figure 13(a–d) and 14(a–d) show secondary structure as a function of simulation time determined with DSSP.

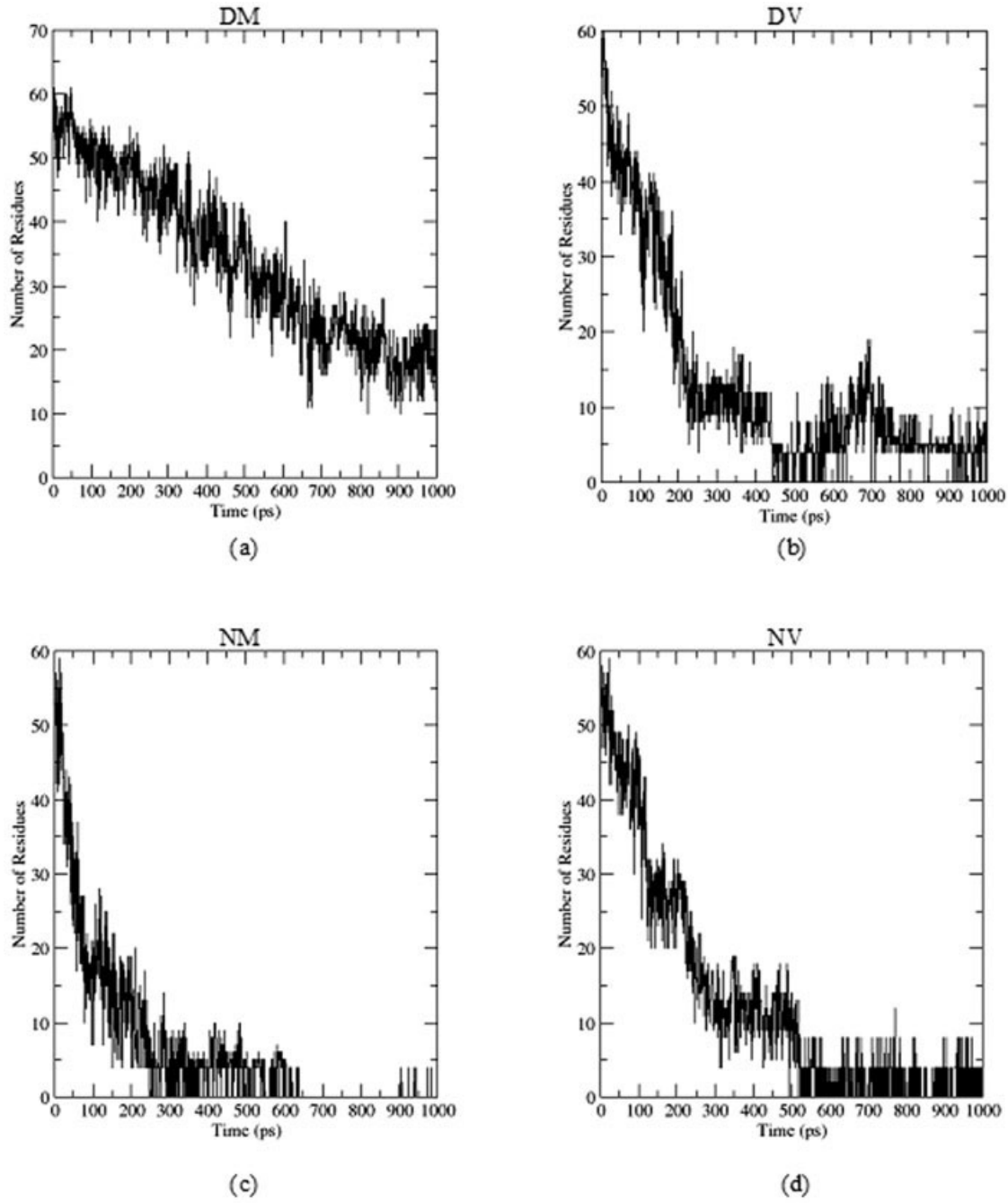

Fig. 13. Secondary structure (helices) as a function of simulation time determined with DSSP at 500K: (**a**) DM, (**b**) DV, (**c**) NM, (**d**) NV.

DM showed an almost constant unwinding movement rate, with the helices unwinding from the C-terminal end [Fig. 5(a)]. Helix content was reduced from 62 to 3% [Fig. 13(a)]. There was no increase of β-sheet content in DM throughout the simulation. DV and both D178N mutants showed faster dissolution of helices, with their α-helix contents falling to less than 10% within 0.3 ns. Interestingly, there was an overall increase of β-sheet content in these variants. The β-sheet content increased from 7 to 16% for DV, 7% to as much as 19% for NM, and 7 to 17% for NV. The highest increase occurred in NM but fluctuated throughout the simulation. In contrast, β-sheet content in NV was stable throughout the simulation. This is contrary to previous experimental results that have suggested a higher propensity for Met at c129 to form sheets.[15]

Distances Between Tyr128 and Asp/Asn178

Substitution of Asp 178 with Asn in NM and NV affects a solvent-accessible bridge of Arg164 (S2) to Asp178 (H2)

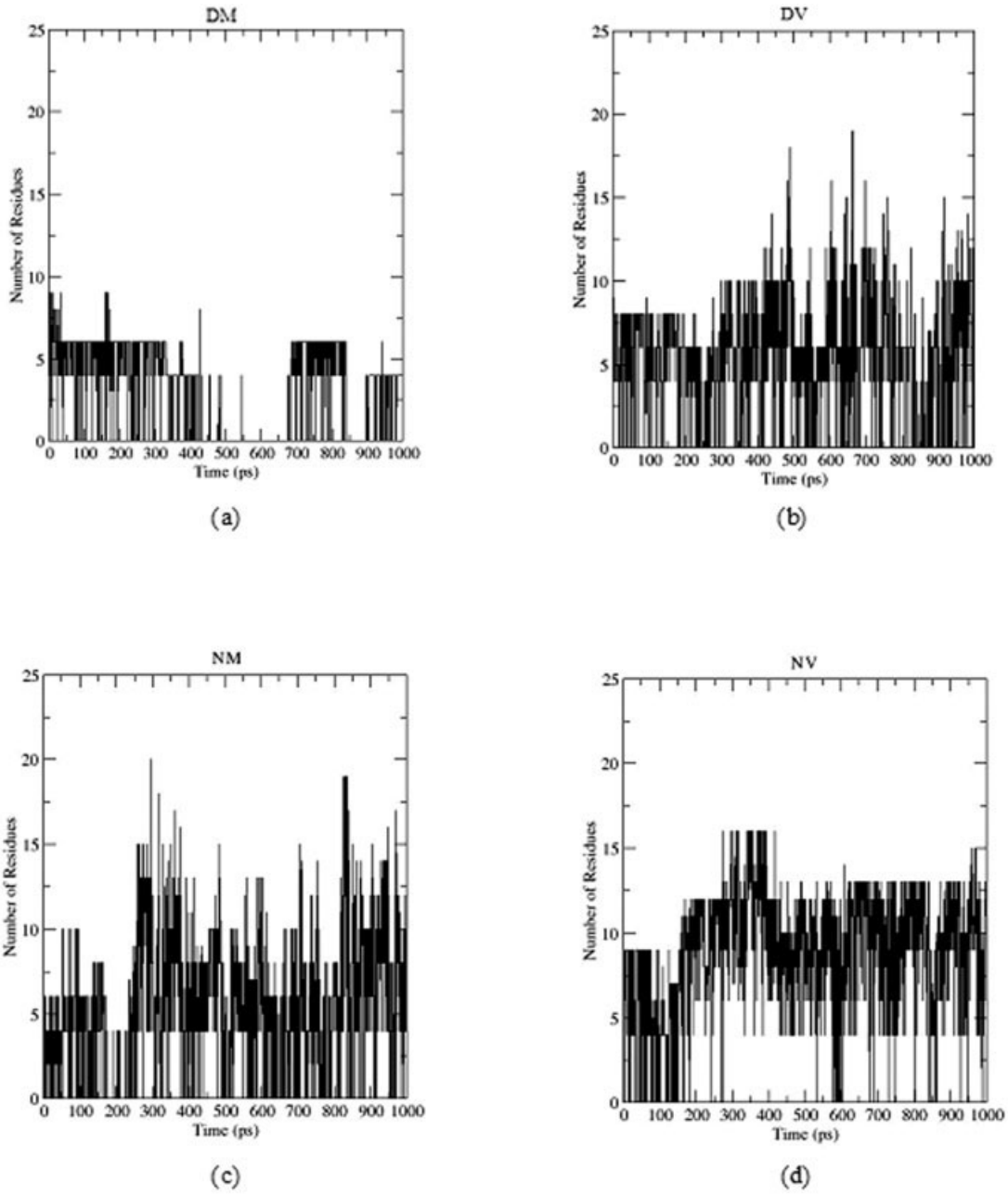

Fig. 14. Secondary structure (β-sheets) as a function of simulation time determined with DSSP at 500K: (**a**) DM, (**b**) DV, (**c**) NM, (**d**) NV.

and a hydrogen bond between Tyr128 (S1) and Asp 178 (H2). The absence of this hydrogen bond in D178N mutants should cause an increase in the dynamics and contribute to the conformational rearrangement between β-sheets and H2 [Fig. 3(e)]. The distances between Tyr128 and Asp/Asn178 were measured during the simulations to determine if D178N mutation would cause the distance to increase, indicating a structural change.

During the simulation at 300K, the distance between the two residues in DM fluctuated within 0.25 nm, indicating no significant movement between β-sheets and H2. In contrast, the distance between the two residues in NM increased by more than 0.25 nm, indicating that the absence of hydrogen bonds contributes to increased mobility of the β-sheets. There was no difference in the distance values between DV and NV at 300K, demonstrating that in the case of valine polymorphic variants, the loss of hydrogen bond does not cause any significant differences in the mobility of β-sheets.

At 500K, there was a higher distance fluctuation in all the variants, with NM increasing up to ten-times the distance at 300K. DM, DV and NV showed only limited distance fluctuations similar to those of NM at 300K. This restriction of mobility can be credited the presence of bonding between Asp178 and Tyr 128 in the wildtype.

However, even though the absence of bonding in mutants should increase fluctuations, the lack of fluctuations in NV are attributed to the formation of β-sheets between the now denatured H2 and the existing beta-sheets [Fig. 9(c)]. In the absence of such restrictive structure formation, as exemplified in NM [Fig. 8(c)], absence of a hydrogen bond between Tyr128 and Asp178 in the mutant increased mobility of β-sheets. The absence of hydrogen bonds in D178N mutants would provide an opportunity for greater mobility between S1 and H2. However, it did not result in altered dynamics during simulations at 300K. This suggests that D178N mutation would not cause an immediate change in structural conformation under normal conditions.

CONCLUSIONS

This is the first reported study of polymorphic behavior at elevated temperatures using MD simulation to assess whether there are any observable differences between normal and mutant variants of c129 polymorphism. There are no significant differences in the behavior of all variants at 300K. The absence of a hydrogen bond between Asn178 in H2 and Tyr128 in S1 did not cause any altered dynamics in mutant prions in its normal state. This excludes the possibility that D178N mutation intrinsically causes a PrP^{SC}-like conformation and leads to soluble precursors of oligomeric PrP^{SC} and suggests that the disease-causing properties are evident in the dynamics or unfolding of the proteins. Simulations also demonstrated a difference in stability and rigidity between Met and Val polymorphic variants that suggests a specific role for Met/Val in the stability and dynamics of PrP^{C} and D178N mutants. Our results show that rapid denaturation of H1 occurred in all variants, with the slowest rate observed in DM, thus confirming the previously reported view that H1 is the least stable helix. Results also show the elongation of existing β-sheets and the formation of new β-sheets occurring more readily in mutant variants, which indicates a higher propensity for mutants to form structures with increased β-sheet content. Efforts are ongoing to perform longer simulations of human prion and its mutants to gain a better understanding of them and to help elucidate the underlying mechanism(s) of conformational change from PrP^{C} to PrP^{SC}.

REFERENCES

1. Prusiner SB. Molecular biology and pathogenesis of prion diseases. Trends Biochem Sci 1996;21(12):482–487.
2. Endo T, Groth D, Prusiner SB, Kobata A. Diversity of oligosaccharide structures linked to asparagines of the scrapie prion protein. Biochemistry 1989;28(21):8380–8388.
3. Turk E, Teplow DB, Hood LE, Prusiner SB. Purification and properties of the cellular and scrapie hamster prion proteins. Eur J Biochem 1988;176(1):21–30.
4. Stahl N, Baldwin MA, Hecker R, Pan KM, Burlingame AL, Prusiner SB. Glycosylinositol phospholipid anchors of the scrapie and cellular prion proteins contain sialic-acid. Biochemistry 1992; 31(21):5043–5053.
5. Brown DR, Sassoon J. Copper-dependent functions for the prion protein. Mol Biotechnol 2002;22(2):165–178.
6. Klamt F, Dal-Pizzol F, da Frota MLC, Walz R, Andrades ME, da Silva EG, Brentani RR, Izquierdo I, Moreira JCF. Imbalance of antioxidant defense in mice lacking cellular prion protein. Free Radic Biol Med 2001;30(10):1137–1144.
7. Shyng SL, Moulder KL, Lesko A, Harris DA. The N-terminal domain of a glycolipid-anchored prion protein is essential for its endocytosis via clathrin-coated pits. J Biol Chem 1995;270(24): 14793–14800.
8. Vey M, Pilkuhn S, Wille H, Nixon R, Dearmond SJ, Smart EJ, Anderson RGW, Taraboulos A, Prusiner SB. Subcellular colocalization of the cellular and scrapie prion proteins in caveolae-like membranous domains. Proc Natl Acad Sci USA 1996;93(25):14945–14949.
9. Tompa P, Friedrich P. Prion proteins as memory molecules: An hypothesis. Neuroscience 1998;86(4):1037–1043.
10. Martins VR, Linden R, Prado MAM, Walz R, Sakamoto AC, Izquierdo I, Brentani RR. Cellular prion protein: on the road for functions. FEBS Lett 2002;512(1–3):25–28.
11. Chiarini LB, Freitas ARO, Martins VR, Brentani RR, Linden R. Neuroprotection mediated by the cellular prion protein. Mol Biol Cell 2000;11:1729.
12. Pearl FMG, Bennett CF, Bray JE, Harrison AP, Martin N, Shepherd A, Sillitoe I, Thornton J, Orengo CA. The CATH database: an extended protein family resource for structural and functional genomics. Nucleic Acids Research 2003;31(1):452–455.
13. Zahn R, Guntert P, von Schroetter C, Wuthrich K. NMR structure of a variant human prion protein with two disulfide bridges. J Mol Biol 2003;326(1):225–234.
14. Zahn R, Liu AZ, Luhrs T, Riek R, von Schroetter C, Garcia FL, Billeter M, Calzolai L, Wider G, Wuthrich K. NMR solution structure of the human prion protein. Proc Natl Acad Sci USA 2000;97(1):145–150.
15. Petchanikow C, Saborio GP, Anderes L, Frossard MJ, Olmedo MI, Soto C. Biochemical and structural studies of the prion protein polymorphism. FEBS Lett 2001;509(3):451–456.
16. Pan KM, Baldwin M, Nguyen J, Gasset M, Serban A, Groth D, Mehlhorn I, Huang ZW, Fletterick RJ, Cohen FE, Prusiner SB. Conversion of alpha-helices into beta-sheets features in the formation of the scrapie prion proteins. Proc Natl Acad Sci USA 1993;90(23):10962–10966.
17. Borchelt DR, Scott M, Taraboulos A, Stahl N, Prusiner SB. Scrapie and cellular prion proteins differ in their kinetics of synthesis and topology in cultured-cells. J Neuropathol Exp Neurol 1990;49(3):311–311.
18. Choi SI, Ju WK, Choi EK, Kim J, Lea HZ, Carp RI, Wisniewski HM, Kim YS. Mitochondrial dysfunction induced by oxidative stress in the brains of hamsters infected with the 263 K scrapie agent. Acta Neuropathol 1998;96(3):279–286.
19. Kim NH, Park SJ, Jin JK, Kwon MS, Choi EK, Carp RI, Kim YS. Increased ferric iron content and iron-induced oxidative stress in the brains of scrapie-infected mice. Brain Res 2000;884(1-2):98–103.
20. Florio T, Grimaldi M, Scorziello A, Salmona M, Bugiani O, Tagliavini F, Forloni G, Schettini G. Intracellular calcium rise through L-type calcium channels, as molecular mechanism for prion protein fragment 106–126-induced astroglial proliferation. Biochem Biophys Res Commun 1996;228(2):397–405.
21. Florio T, Thellung S, Amico C, Robello M, Salmona M, Bugiani O, Tagliavini F, Forloni G, Schettini G. Prion protein fragment 106–126 induces apoptotic cell death and impairment of L-type voltage-sensitive calcium channel activity in the GH3 cell line. J Neurosci Res 1998;54(3):341–352.
22. Giese A, Groschup MH, Hess B, Kretzschmar HA. Neuronal cell-death in scrapie-infected mice is due to apoptosis. Brain Pathol 1995;5(3):213–221.
23. Lucassen PJ, Williams A, Chung WCJ, Fraser H. Detection of apoptosis in murine scrapie. Neurosci Lett 1995;198(3):185–188.
24. Fairbairn DW, Carnahan KG, Thwaits RN, Grigsby RV, Holyoak GR, Oneill KL. Detection of apoptosis induced DNA cleavage in scrapie-infected sheep brain. FEMS Microbiol Lett 1994;115(2-3): 341–346.
25. Solforosi L, Criado JR, McGavern DB, Wirz S, Sanchez-Alavez M, Sugama S, DeGiorgio LA, Volpe BT, Wiseman E, Abalos G, Masliah E, Gilden D, Oldstone MB, Conti B, Williamson RA. Cross-linking cellular prion protein triggers neuronal apoptosis in vivo. Science 2004;303(5663):1514–1516.
26. Kim BH, Lee HG, Choi JK, Kim JI, Choi EK, Carp RI, Kim YS. The cellular prion protein (PrPC) prevents apoptotic neuronal cell death and mitochondrial dysfunction induced by serum deprivation. Molecular Brain Research 2004;124(1):40–50.
27. Goldfarb LG, Petersen RB, Tabaton M, Brown P, Leblanc AC,

Montagna P, Cortelli P, Julien J, Vital C, Pendelbury WW, Haltia M, Wills PR, Hauw JJ, McKeever PE, Monari L, Schrank B, Swergold GD, Autiliogambetti L, Gajdusek DC, Lugaresi E, Gambetti P. Fatal familial insomnia and familial Creutzfeldt-Jakob disease – disease phenotype determined by a DNA polymorphism. Science 1992;258(5083):806–808.
28. Chen SG, Parchi P, Brown P, Capellari S, Zou WQ, Cochran EJ, VnencakJones CL, Julien J, Vital C, Mikol J, Lugaresi E, AutilioGambetti L, Gambetti P. Allelic origin of the abnormal prion protein isoform in familial prion diseases. Nat Med 1997;3(9):1009–1015.
29. Collinge J. Human prion diseases. Brain Pathol 2000;10(4):607.
30. Knight R. Variant CJD: the present position and future possibilities. Int J Pediatr Otorhinolaryngol 2003;67:S81–S84.
31. Monari L, Petersen RB, Chen SG, Cortelli P, Montagna P, Berg L, Julien J, Lugaresi E, AutilioGambetti L, Gambetti P. Detection of prion protein in fibroblasts from 2 Fatal familial insomnia kindred. J Neuropathol Exp Neurol 1993;52(3):293.
32. Palmer MS, Dryden AJ, Hughes JT, Collinge J. Homozygous prion protein genotype predisposes to sporadic Creutzfeldt-Jakob disease. Nature 1991;352(6333):340–342.
33. Will RG. Variant Creutzfeldt–Jakob disease. Acta Neurobiol Exp 2002;62(3):167–173.
34. Gambetti P, Medori R, Tritschler H, Leblanc A, Montagna P, Cortelli P, Tinuper P, Monari L, Tabaton M, Petersen R, AutilioGambetti L, Lugaresi E. Fatal familial insomnia (Ffi) – a prion disease with a mutation at codon-178 of the prion protein gene. J Neuropathol Exp Neurol 1992;51(3):353.
35. Petersen RB, Parchi P, Richardson SL, Urig CB, Gambetti P. Effect of the D178N mutation and the codon 129 polymorphism on the metabolism of the prion protein. J Biol Chem 1996;271(21):12661–12668.
36. Collins S, McLean CA, Masters CL. Gerstmann-Straussier-Scheinker syndrome, fatal familial insomnia, and kuru: a review of these less common human transmissible spongiform encephalopathies. J Clin Neurosci 2001;8(5):387–397.
37. Day R, Bennion BJ, Ham S, Daggett V. Increasing temperature accelerates protein unfolding without changing the pathway of unfolding. J Mol Biol 2002;322(1):189–203.
38. Santini S, Claude JB, Audic S, Derreumaux P. Impact of the tail and mutations G131V and M129V on prion protein flexibility. Proteins 2003;51(2):258–265.
39. Gsponer J, Ferrara P, Caflisch A. Flexibility of the murine prion protein and its Asp178Asn mutant investigated by molecular dynamics simulations. J Mol Graph 2001;20(2):169–182.
40. Zou WQ, Capellari S, Parchi P, Sy MS, Gambetti P, Chen SG. Identification of novel proteinase K-resistant C-terminal fragments of PrP in Creutzfeldt-Jakob disease. J Biol Chem 2003;278(42):40429–40436.
41. Berman HM, Battistuz T, Bhat TN, Bluhm WF, Bourne PE, Burkhardt K, Iype L, Jain S, Fagan P, Marvin J, Padilla D, Ravichandran V, Schneider B, Thanki N, Weissig H, Westbrook JD, Zardecki C. The Protein Data Bank. Acta Crystallogr D Biol Crystallogr 2002;58:899–907.
42. Guex N, Peitsch MC. SWISS-MODEL and the Swiss-PdbViewer: An environment for comparative protein modeling. Electrophoresis 1997;18(15):2714–2723.
43. Herrmann LM, Caughey B. The importance of the disulfide bond in prion protein conversion. Neuroreport 1998;9(11):2457–2461.
44. Lindahl E, Hess B, van der Spoel D. GROMACS 3.0: a package for molecular simulation and trajectory analysis. J Molecular Modeling 2001;7(8):306–317.
45. Gu W, Wang TT, Zhu J, Shi YY, Liu HY. Molecular dynamics simulation of the unfolding of the human prion protein domain under low pH and high temperature conditions. Biophys Chem 2003;104(1):79–94.
46. El-Bastawissy E, Knaggs MH, Gilbert IH. Molecular dynamics simulations of wild-type and point mutation human prion protein at normal and elevated temperature. J Mol Graph 2001;20(2):145–154.
47. Taylor DM. Inactivation of TSE agents: safety of blood and blood-derived products. Transfu Clin Biol 2003;10(1):23–25.
48. Brown P, Meyer R, Cardone F, Pocchiari M. Ultra-high-pressure inactivation of prion infectivity in processed meat: A practical method to prevent human infection. Proc Natl Acad Sci USA 2003;100(10):6093–6097.
49. Kabsch W, Sander C. Dictionary of protein secondary structure – pattern-recognition of hydrogen-bonded and geometrical features. Biopolymers 1983;22(12):2577–2637.
50. Sayle RA, Milnerwhite EJ. Rasmol – biomolecular graphics for all. Trends Biochemical Sciences 1995;20(9):374–376.
51. Martz E. Protein explorer: easy yet powerful macromolecular visualization. Trends Biochemical Sciences 2002;27(2):107–109.
52. Guilbert C, Ricard F, Smith JC. Dynamic simulation of the mouse prion protein. Biopolymers 2000;54(6):406–415.
53. Alonso DOV, DeArmond SJ, Cohen FE, Daggett V. Mapping the early steps in the pH-induced conformational conversion of the prion protein. Proc Natl Acad Sci USA 2001;98(6):2985–2989.
54. Liemann S, Glockshuber R. Influence of amino acid substitutions related to inherited human prion diseases on the thermodynamic stability of the cellular prion protein. Biochemistry 1999;38(11):3258–3267.
55. Prusiner SB. Prions. Proc Natl Acad Sci USA 1998;95(23):13363–13383.
56. Pappalardo M, Milardi D, La Rosa C, Zannoni C, Rizzarelli E, Grasso D. A molecular dynamics study on the conformational stability of PrP 180–193 helix II prion fragment. Chem Phys Lett 2004;390(4–6):511–516.
57. Morrissey MP, Shakhnovich EI. Evidence for the role of PrPC helix 1 in the hydrophilic seeding of prion aggregates. Proc Natl Acad Sci USA 1999;96(20):11293–11298.
58. Speare JO, Rush TS, Bloom ME, Caughey B. The role of helix 1 aspartates and salt bridges in the stability and conversion of prion protein. J Biol Chem 2003;278(14):12522–12529.
59. Kim CWA, Berg JM. Thermodynamic beta-sheet propensities measured using a zinc-finger host peptide. Nature 1993;362(6417):267–270.
60. Smith CK, Withka JM, Regan L. A thermodynamic scale for the beta-sheet forming tendencies of the amino-acids. Biochemistry 1994;33(18):5510–5517.
61. Milnerwhite EJ, Poet R. Loops, bulges, turns and hairpins in proteins. Trends Biochemical Sciences 1987;12(5):189–192.
62. Li SC, Goto NK, Williams KA, Deber CM. Alpha-helical, but not beta-sheet, propensity of proline is determined by peptide environment. Proc Natl Acad Sci USA 1996;93(13):6676–6681.
63. Dima RI, Thirumalai D. Exploring the propensities of helices in PrPc to form beta sheet using NMR structures and sequence alignments. Biophys J 2002;83(3):1268–1280.
64. Mornon JP, Prat K, Dupuis F, Callebaut I. Structural features of prions explored by sequence analysis I. Sequence data. Cell Mol Life Sci 2002;59(8):1366–1376.